Dynamic Contrast-Enhanced T1-Weighted Perfusion Magnetic Resonance Imaging Identifies Glioblastoma Immunohistochemical Biomarkers via Tumoral and Peritumoral Approach: A Pilot Study

Kerem Ozturk[1], Esra Soylu[1], Sahsine Tolunay[2], Selin Narter[2], Bahattin Hakyemez[1]

OBJECTIVE: **We aimed to evaluate the usefulness of dynamic contrast-enhanced T1-weighted perfusion magnetic resonance imaging (DCE-pMRI) to predict certain immunohistochemical (IHC) biomarkers of glioblastoma (GB) in this pilot study.**

METHODS: **We retrospectively reviewed 36 patients (male/female, 25:11; mean age, 53 years; age range, 29–85 years) who had pretreatment DCE-pMRI with IHC analysis of their excised GBs. Regions of interest of the enhancing tumor (ER) and nonenhancing peritumoral region (NER) were used to calculate DCE-pMRI parameters of volume transfer constant, back flux constant, volume of the extravascular extracellular space, initial area under enhancement curve, and maximum slope. IHC biomarkers including Ki-67 labeling index, epidermal growth factor receptor (EGFR), oligodendrocyte transcription factor 2 (OLIG2), isocitrate dehydrogenase 1 (IDH1), and p53 mutation status were determined. The imaging metrics of GB with IHC markers were compared using the Kruskal-Wallis test and Spearman correlation analysis.**

RESULTS: **Among 30 patients with available IDH1 status, 14 patients (46.6%) had IDH1 mutation. EGFR amplification was present in 24/36 (66.6%) patients. Mean Ki-67 labeling index was 29% (range, 1.5%–80%). p53 mutation was present in 20/36 GBs (55%), whereas OLIG2 expression was positive in 29/36 GBs (80.5%). Various DCE-pMRI parameters gathered from the ER and NER were significantly correlated with IDH1 mutation, EGFR amplification, and OLIG2 expression ($P < 0.05$). Ki-67 labeling index showed a strong positive correlation with initial area under enhancement curve ($r = 0.619$; $P < 0.001$).**

CONCLUSIONS: **DCE-pMRI could determine surrogate IHC biomarkers in GB via tumoral and peritumoral approach, potential targets for individualized treatment protocols.**

Key words
- Dynamic contrast-enhanced T1-weighted perfusion MR imaging (DCE-pMRI)
- Epidermal growth factor receptor (EGFR)
- Glioblastoma (GB)
- Isocitrate dehydrogenase 1 (IDH1)
- Oligodendrocyte transcription factor 2 (OLIG2)

Abbreviations and Acronyms
AUC: Area under the curve
DCE-pMRI: Dynamic contrast-enhanced T1-weighted perfusion magnetic resonance imaging
EES: Extravascular extracellular space
EGFR: Epidermal growth factor receptor
ER: Enhancing tumoral region
FLAIR: Fluid-attenuated inversion recovery
FOV: Field of view
GB: Glioblastoma
iAUC: Initial area under enhancement curve
IDH1: Isocitrate dehydrogenase 1
IDH-mut: Isocitrate dehydrogenase 1 mutation–positive
IDH-wt: Without isocitrate dehydrogenase 1 mutation
IHC: Immunohistochemical
Kep: Back flux constant
Ktrans: Volume transfer constant
LOOCV: Leave-one-out cross-validation
MaxSlope: Maximum slope
MRI: Magnetic resonance imaging
NER: Nonenhancing peritumoral T2 hyperintense region
OLIG2: Oligodendrocyte transcription factor 2
ROI: Region of interest
TBV: Tumor blood volume
TE: Echo time
TR: Repetition time
Ve: Volume of the extravascular extracellular space
VEGF: Vascular endothelial growth factor

From the Departments of [1]Radiology and [2]Pathology, Uludag University Faculty of Medicine, Bursa, Turkey

To whom correspondence should be addressed: Bahattin Hakyemez , M.D. [E-mail: bhakyemez@uludag.edu.tr]

Citation: World Neurosurg. (2019) 128:e195-e208.
https://doi.org/10.1016/j.wneu.2019.04.089

*Journal homepage: **www.journals.elsevier.com/world-neurosurgery***

*Available online: **www.sciencedirect.com***

1878-8750/$ - see front matter

INTRODUCTION

Glioblastoma (GB) is the most common primary malignant brain tumor, with a dismal prognosis,[1] usually explained by its molecular genomic variability.[2] According to a recent study by the Cancer Genome Atlas Research Network,[3] GB should not be considered a single disease but rather should be categorized by molecular subtypes, each with different sensitivity to therapy and prognosis. As a consequence, there has been a recent emphasis on defining genetically unique subtypes of GB that might serve as targets of individualized therapy strategies.

Numerous studies have focused on the certain genetic alterations in GBs to further dissect the underlying mechanisms and to contribute to a better prognosis.[4] Over the last decade, several genetic alterations including isocitrate dehydrogenase 1 (IDH1), epidermal growth factor receptor (EGFR), oligodendrocyte transcription factor 2 (OLIG2), and p53 mutation as well as proliferation marker of Ki-67 nuclear labeling index have been identified in GB tissue.[5] One of the most exciting and clinically relevant observations was the discovery that a high percentage of secondary GBs harbor mutations in the IDH1 gene that are associated with increased angiogenesis and better prognosis in GB.[6] The increased Ki-67 nuclear labeling index, which is a cellular protein and associated with the tumoral proliferative activity, carries an unfavorable prognosis.[7] OLIG2 plays a substantial role in the development of glioma.[8] OLIG2 expression—positive glioma cells invade brain tissue without affecting the existing vasculature, whereas OLIG2 expression—negative cells grow as clusters around blood vessels and express high levels of the angiogenic factors.[9] EGFR encodes a transmembrane tyrosine kinase on the cell surface.[10] Dimerization of the receptor initiates numerous signaling cascades that induce cell proliferation and angiogenesis and also inhibit apoptosis.[11] Although such underlying genomic abnormalities have improved the clinical evaluation of GB,[12] there is still an unmet clinical demand for easily accessible imaging biomarkers capable of delineating underlying genetic activities. Therefore, accurate noninvasive characterization of surrogate immunohistochemical (IHC) biomarkers in GB is crucial not only for a better understanding of this poor-prognosis tumor but also for developing individualized treatments to further improve patient outcome.

The use of magnetic resonance imaging (MRI) has recently expanded to create noninvasive imaging biomarkers of molecular alterations in GB.[13,14] Unlike conventional MRI, dynamic contrast-enhanced T1-weighted perfusion MRI (DCE-pMRI) provides insight into the physiologic and hemodynamic characteristics of neoplastic tissue by evaluating tumor vascularity and permeability.[15] DCE-pMRI allows for assessment of the vascular microenvironment in tumors[16] by measurement of a range of quantitative parameters, such as Ktrans (volume transfer constant), Kep (back flux constant), and Ve (volume of the extravascular extracellular space [EES]) as well as semi-quantitative parameters including initial area under enhancement curve (iAUC) and maximum slope (MaxSlope) in the signal intensity-time series curve.[17,18] Although a few studies have attempted to correlate the genetic expression of a tumor with certain morphologic radiologic characteristics,[19,20] no reports, to the best of our knowledge, covering the role of DCE-pMRI in predicting surrogate IHC biomarkers of GB are available.

The goal of this pilot study is to assess the usefulness of DCE-pMRI obtained from the enhancing tumoral region (ER) and nonenhancing peritumoral T2 hyperintense region (NER) to derive robust imaging biomarkers that can be used to identify major IHC markers in GB.

METHODS

Patient Characteristics

Our institutional review board approved this retrospective study, and informed consent was waived. Using a computed search of our hospital's medical records and pathology files from January 2016 to June 2018, we identified 44 patients who had preoperative DCE-pMRI with IHC analysis and histopathologic diagnosis of GB. We included patients with available pretreatment DCE-pMRI with matching postcontrast axial T1-weighted and fluid-attenuated inversion recovery (FLAIR) T2-weighted images and surgical resection with sufficient tumor tissue for IHC analysis. None of the patients had received previous or concurrent radiotherapy or chemotherapy. We excluded a patient who was on steroid therapy. An additional 7 patients, 3 with no IHC results, 2 with a pathologic diagnosis via stereotactic biopsy; 1 with severe paramagnetic artifacts, and 1 with motion artifacts on MRI, were also excluded. The flow diagram of patient selection and exclusion is shown in **Figure 1**.

A total of 36 patients (male/female, 25:11; mean age, 53 years; age range, 29—85 years) met the outlined inclusion and exclusion criteria and served as the final cohort. Above all, the results of the IDH1 mutation analysis of 6 patients were excluded from the study because of the problems of quality assessment and standardization during the first implementation of the IHC procedure at our institution in 2016. Therefore, the status of IDH1 mutation was evaluated in 30 patients. All DCE-pMRI examinations were conducted within 2 weeks before the surgery (mean, 6.5 days). Of the 36 patients, 12 underwent gross total resection, 16 had a subtotal resection, and 8 had a partial resection.

Technique

MRI examinations were performed on a 1.5-T scanner (Signa Explorer [GE Medical Systems, Milwaukee, Wisconsin, USA]), equipped with a 16-channel sensitivity-encoding head coil. Patients underwent routine MRI, including T1-weighted spin-echo sequence (field of view [FOV], 230 × 250 mm; section thickness, 4 mm; repetition time [TR]/echo time [TE], 500—580/10—16 milliseconds; flip angle, 90°), T2-weighted fast spin-echo sequence (FOV, 230 × 250 mm; section thickness, 5 mm; TR/TE, 5800—6700/95—115 milliseconds; flip angle, 90°), and FLAIR sequence (FOV, 27—32 cm; section thickness, 4 mm; TR/TE, 6000—7000/90—105 milliseconds; inversion time, 2100).

DCE-pMRI was performed with a T1-weighted spoiled saturation recovery gradient echo sequence covering 4 slices over the center of the tumor. The following parameters were used: TR/TE, 7.1/4.2 milliseconds; flip angle, 15°; matrix, 96 × 96; FOV, 24 × 24 cm; section thickness, 3.6 mm; in-plane acquisition voxel size,

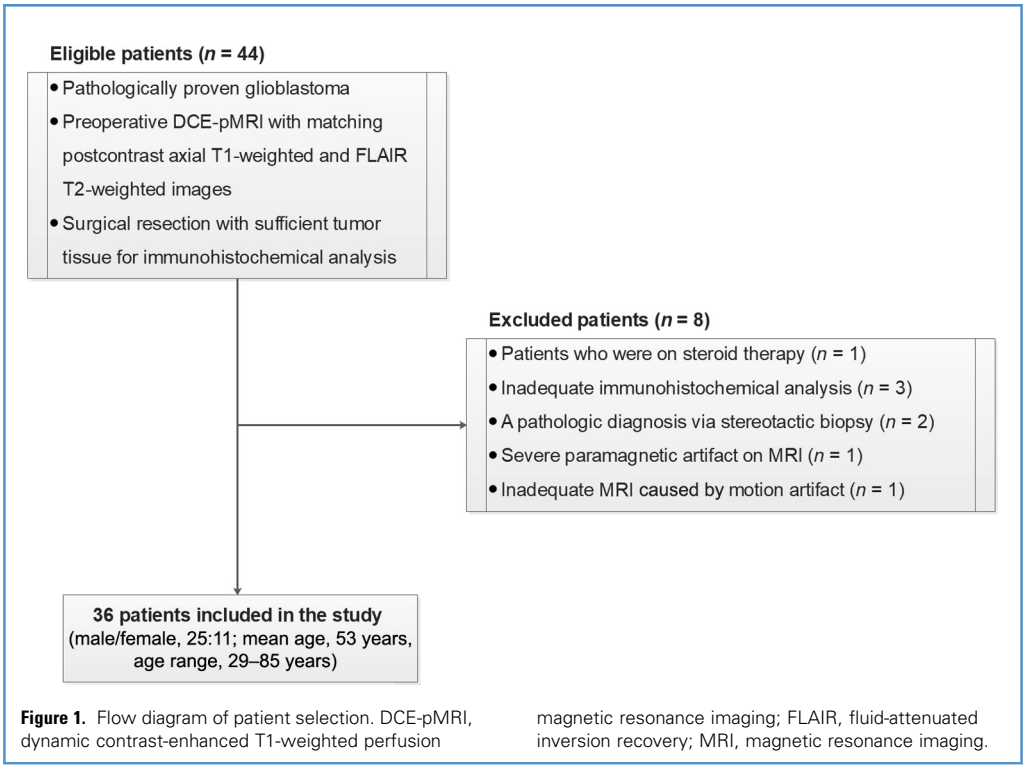

Figure 1. Flow diagram of patient selection. DCE-pMRI, dynamic contrast-enhanced T1-weighted perfusion magnetic resonance imaging; FLAIR, fluid-attenuated inversion recovery; MRI, magnetic resonance imaging.

0.9 × 0.9 mm. Imaging was performed with a standard 0.1 mmol/kg body weight dose of gadolinium-based contrast agent of gadobenate dimeglumine (Dotarem [Guerbet, Aulnay-sous-Bois, France]). The gadolinium-based contrast agent was administered through a catheter in the antecubital vein by an automatic power injector (Medrad, Pittsburgh, Pennsylvania, USA) at a rate of 3 mL/second and was followed by a double bolus injection of isotonic saline. The dynamic acquisition was performed with a temporal resolution of 3.52 seconds, and the contrast agent was administered after 10 baseline dynamics (total, 120 dynamic images). After the pMRI, contrast-enhanced T1-weighted spin-echo sequences were conducted on axial, coronal, and sagittal planes.

Image Analysis

The conventional MRIs and DCE-pMRI were digitally transferred to a dedicated workstation (AW VolumeShare 7 [GE Medical Systems, Milwaukee, Wisconsin, USA]) for postprocessing (GenIQ Brain [GE Medical Systems, Milwaukee, Wisconsin, USA]) for further analysis. Postprocessing such as motion correction of dynamic images, a vascular input function, T1 mapping with different flip angles, registration of pixels on a T1 map, and pharmacokinetic modeling was automatically conducted. Two investigators (K.O. and E.S., with 4 years and 6 years of neuroradiology experience, respectively), who were blinded to the clinical data and molecular subtypes of tumors, carefully drew at least 0.5 cm^2 3-circle regions of interest (ROIs) involving the highest color levels of the solid portions of tumoral lesion (ER) on parametric maps with reference to conventional MRIs and their average values were recorded. Because the ROI placement was conducted on the parametric maps coregistered with structural images, the margin of the lesions could be defined with confidence. The ROIs were carefully positioned to avoid cystic or necrotic parts and large vessels according to the combined data from the T1-weighted image and T2 FLAIR image. To reduce confounding factors, ROI sizes were kept constant for each lesion. NER was defined as a region clearly outside the well-defined solid portion, absolutely containing no enhancement, and high signal intensity on T2-weighted and FLAIR images. NER was selected because this immediate area around the contrast-enhancing region is known to possess potentially clinically relevant regions of tumor invasion. For the NER, 3 uniform ROIs of minimum 0.5 cm^2 were drawn at the center of the portion where the T2-signal abnormality was noted after careful inspection of T1-weighted and T2-weighted images and their average values were recorded. The ROIs were localized at least 5 mm away from the area enhancing after contrast administration, avoiding points in the enhancing tumor tissue. All ROIs were verified and supervised by an expert board-certified neuroradiologist (B.H., with 20 years of neuroimaging experience).

The maps of pharmacokinetic parameters, including Ktrans, Ve, and Kep were determined with the extended 2-compartment pharmacokinetic Tofts and Kermode model.[21] The linear assumption was performed between the change in signal intensity and gadolinium concentration for converting the signal intensity curve to a concentration-time curve. iAUC values were acquired by integrating the area under the time-to-signal-intensity curve, from 0 to 60 seconds after contrast agent arrival on the basis of previous studies. MaxSlope was defined as the MaxSlope in the time-to-signal-intensity curve of each voxel. iAUC and MaxSlope values were automatically calculated without any user-

dependent input, to maximize interrater reliability, through automatic determination of the time of contrast agent arrival for each pixel.

IHC and Morphometric Analysis

The IHC profile was obtained from paraffin-embedded specimens with hematoxylin-eosin staining by experienced neuropathologists. For IDH1, EGFR, and OLIG2 staining, the binomial classification of "positive" or "negative" was used. Nuclear staining of p53 mutation was scored semi-quantitatively in the most prominently stained area of the tissue slides. The Ki-67 labeling index was identified by the areas of greatest tumor cellularity, analyzing a minimum of 10 fields at 400× (high-power) magnification on an Olympus microscope (Olympus America Inc., Center Valley, Pennsylvania, USA). An Aperio image analyzer (Aperio Technologies, Vista, California, USA) was used to evaluate the expression status of p53 mutation. The types of cells labeled by p53 IHC methods and a semi-quantification of general numbers of tumor cells labeled were recorded as a continuous variable. A focal and diffuse positive staining for p53 positivity expression status was scored as positive as a factor for studying the DCE-pMRI parameters. Technical specifications of antibodies used for IHC analyses are shown in Table 1.

Statistical Analysis

Statistical analysis was performed with a commercially available statistical software package (SPSS, version 23.0 for Windows [IBM Corp., Armonk, New York, USA]). Descriptive statistics are presented for a continuous variable; count and percent are reported for a categorical variable. Because of the small sample size, we used nonparametric statistical analysis.

The mean and standard deviation of each DCE-pMRI measurement for tumors were obtained. The associations between each measurement were assessed through Spearman rank correlation coefficients. Group comparisons of DCE-pMRI imaging variables (Ktrans, Vep, Kep, area under the curve [AUC], and MaxSlope) of patients with various molecular markers (EGFR amplification, OLIG2 expression, IDH1 mutation, p53 mutation, and Ki-67 labeling index status) were performed using the Kruskal-Wallis test, and a Dunn test was used for post hoc comparisons. Corrections for multiple comparisons were performed using the Bonferroni correction method. Spearman correlation analysis was performed to measure the significance of the association between the DCE-pMRI parameters and semi-quantitatively determined p53 mutation status, as well as Ki-67 labeling index.

The predictive potential of each imaging parameter was analyzed using the area under the receiver operating characteristic curve in both ER and NER, separately. The sensitivity and specificity of the suggested cutoff values were calculated using the Youden statistic to evaluate the diagnostic performance, and the cutoff value with the best diagnostic performance (highest sensitivity and specificity) for each parameter was determined. Among the identified DCE-pMRI parameters, the one with the largest AUC on receiver operating characteristic curve was validated by using the leave-one-out cross-validation (LOOCV) test in predicting the IHC alterations in GB. In each validation round, 1 patient was selected as a testing sample, and the remaining patients were used as training samples. On the basis of the result of all rounds, the cutoff value was validated using sensitivity and specificity.

The interobserver correlation between the 2 observers' mean ROI measurements was tested using the Lin concordance correlation coefficient. Intraobserver agreements for quantitative imaging parameters were assessed with the intraclass correlation coefficient.

In all tests, P values <0.05 were considered statistically significant.

RESULTS

A total of 36 patients had preoperative conventional MRI and DCE-pMRI data suitable for evaluation. There was no significant difference in gender and age between the different molecular profiles of the GB ($P > 0.05$).

Among 30 patients with available IDH1 status, positive immunoreactivity to IDH1 was noted in 46.6% of patients (14/30) (considered as IDH1 mutation positive [IDH-mut]). EGFR amplification was present in 24 patients (66.6%). Mean Ki-67 labeling index was 29% (range, 1.5%–80%). P53 mutation was present in 20/36 (55%) and mean number (%) p53-mutation immunoreactive cells in GBs was 18% (range, 0%–90%). OLIG2 amplification was detected in 29/36 tumors (80%). One representative case of IDH-mut GB is presented in Figure 2.

IDH1 Mutation

The Ve and iAUC parameters of the GB subgroup without IDH mutation (IDH-wt) in the ER were significantly higher than those of the IDH-mut GBs (after Bonferroni correction by a factor of 5, Ve, $P = 0.01$; iAUC, $P = 0.05$) (Table 2 and Figure 3A). In terms of Kep, Ktrans, and MaxSlope parameters gathered from ER, we found no significant difference between IDH-mut and IDH-wt GBs ($P > 0.05$).

Table 1. Technical Specifications of Antibodies Used for Immunohistochemical Analyses

Primary Antibody	Identifier	Type	Dilution	Manufacturer
Isocitrate dehydrogenase 1	H09	Mouse monoclonal	1/20	Dianova, Hamburg, Germany
Epidermal growth factor receptor	EP-22	Rabbit monoclonal	1/100	Cell Marque, Rockling, California, USA
Oligodendrocyte transcription factor 2	EP112	Rabbit monoclonal	1/250	Cell Marque, Rockling, California, USA
p53	D0-7	Mouse monoclonal	1/800	Leica Biosystems, Wetzlar, Germany
Ki-67 labeling index	SP6	Rabbit monoclonal	1/250	Cell Marque, Rockling, California, USA

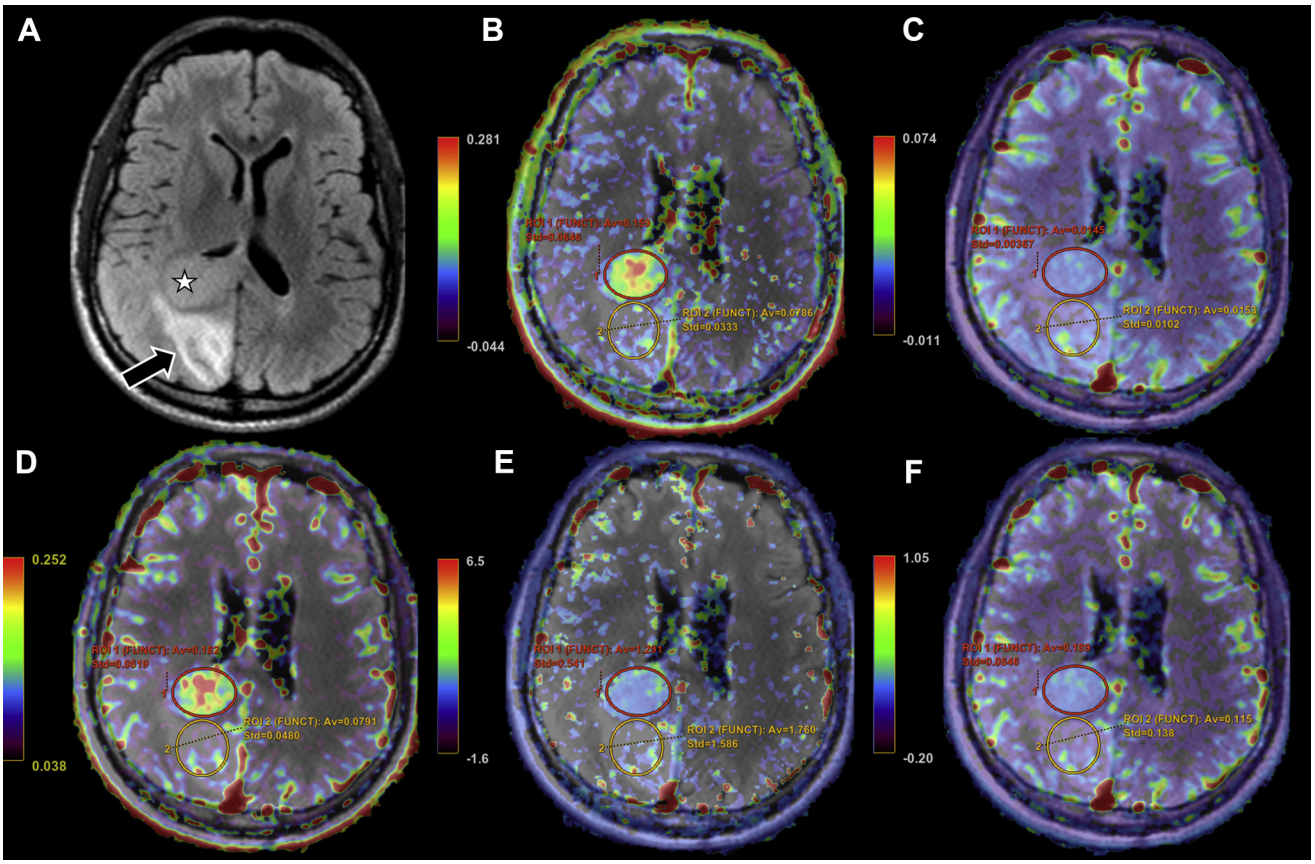

Figure 2. Axial fluid-attenuated inversion recovery T2-weighted magnetic resonance imaging (**A**) showing a solid tumor in the right occipital lobe (*asterisk*) with nonenhancing T2-hyperintense peritumoral edema (*arrow*). Representative dynamic contrast-enhanced T1-weighted perfusion magnetic resonance images and parametric maps from a patient with isocitrate dehydrogenase 1 mutation–positive and epidermal growth factor receptor expression–positive glioblastoma. Corresponding volume of the extravascular extracellular space (**B**), maximum slope (**C**), initial area under enhancement curve (**D**), back flux constant (**E**), and volume transfer constant (**F**) maps show increased perfusion and leakiness on the enhancing tumoral region (*red regions of interest*) and nonenhancing peritumoral T2 hyperintense region (*yellow regions of interest*) of the tumor.

For the ER, the discriminative power of our individual imaging biomarkers was highest for Ve, with an AUC of 0.826 (Figure 3B). The IDH-mut GBs could be differentiated from IDH-wt GBs by using Ve $\leq$ 0.3416, with sensitivity and specificity of 68.8 and 92.9%, respectively. According to the LOOCV of the Ve, the cross-validated sensitivity and specificity in the prediction of IDH1 mutation were 65.7% and 78.6%, respectively.

For NER, $MaxSlope_{NER}$, Ve_{NER}, and $iAUC_{NER}$ parameters of the IDH-wt GB were significantly higher than those of the IDH-mut GBs (after Bonferroni correction by a factor of 5, $MaxSlope_{NER}$, $P = 0.005$; Ve_{NER}, $P = 0.02$; $iAUC_{NER}$, $P = 0.035$) (Table 2 and Figure 4A), whereas there was no significant difference ($P > 0.05$) between IDH-mut and IDH-wt GBs with respect to the Kep_{NER}, and $Ktrans_{NER}$ values.

For the NER, the discriminative power of our individual imaging biomarkers was highest for $MaxSlope_{NER}$, with an AUC of 0.853 (Figure 4B). The IDH-mut GBs could be differentiated from IDH-wt GBs by using $MaxSlope_{NER} \leq 0.0174$, with sensitivity and specificity of 75% and 92.9%, respectively. According to the LOOCV of the $MaxSlope_{NER}$, the cross-validated sensitivity and specificity in the prediction of IDH1 mutation were 72.3% and 86.3%, respectively.

EGFR Amplification

The iAUC and Ve parameters of the GBs with EGFR amplification in the ER were significantly higher than those of the subgroup without EGFR amplification (after Bonferroni correction by a factor of 5, iAUC, $P = 0.005$; Ve, $P = 0.025$) (Table 3 and Figure 5A). In terms of Kep, Ktrans, and MaxSlope parameters gathered from ER, we found no significant difference between the groups with EGFR amplification and without EGFR amplification (all $P > 0.05$).

For the ER, the discriminative power of our individual imaging biomarkers was highest for iAUC, with an AUC of 0.840 (Figure 5B). The GB with EGFR amplification could be differentiated from those without EGFR amplification by using

Table 2. Analysis of the Relationship Between Baseline Perfusion Parameters and Isocitrate Dehydrogenase 1 Mutation Status

Isocitrate Dehydrogenase 1 Mutation Status		Dynamic Contrast-Enhanced T1-Weighted Perfusion Magnetic Resonance Imaging Parameters									
		Initial Area Under Enhancement Curve	Initial Area Under Enhancement Curve Peritumoral Nonenhancing Region	Back Flux Constant (/minute)	Back Flux Constant Peritumoral Nonenhancing Region (/minute)	Volume Transfer Constant (/minute)	Volume Transfer Constant Peritumoral Nonenhancing Region (/minute)	Maximum Slope in Signal Intensity-Time Series Curve (/minute)	Maximum Slope Peritumoral Nonenhancing Region (/minute)	Volume of the Extravascular Extracellular Space (%)	Volume of the Extravascular Extracellular Space Peritumoral Nonenhancing Region (%)
−						N (n = 16)					
	Median	**0.303**	**0.161**	0.817	0.761	0.251	0.117	0.028	**0.021**	**0.389**	**0.194**
	Standard deviation	**0.173**	**0.084**	0.572	0.522	0.156	0.099	0.020	**0.009**	**0.181**	**0.113**
	Range	**0.667**	**0.304**	2.006	1.726	0.638	0.258	0.074	**0.031**	**0.551**	**0.431**
+						N (n = 14)					
	Median	**0.149**	**0.065**	1.071	0.605	0.138	0.069	0.016	**0.013**	**0.130**	**0.073**
	Standard deviation	**0.124**	**0.071**	0.632	0.572	0.184	0.084	0.021	**0.006**	**0.128**	**0.072**
	Range	**0.409**	**0.228**	2.263	1.603	0.610	0.327	0.076	**0.027**	**0.458**	**0.234**

Bold values mean *P* values of those parameters were <0.05 according to the Kruskal-Wallis test with Bonferroni correction.

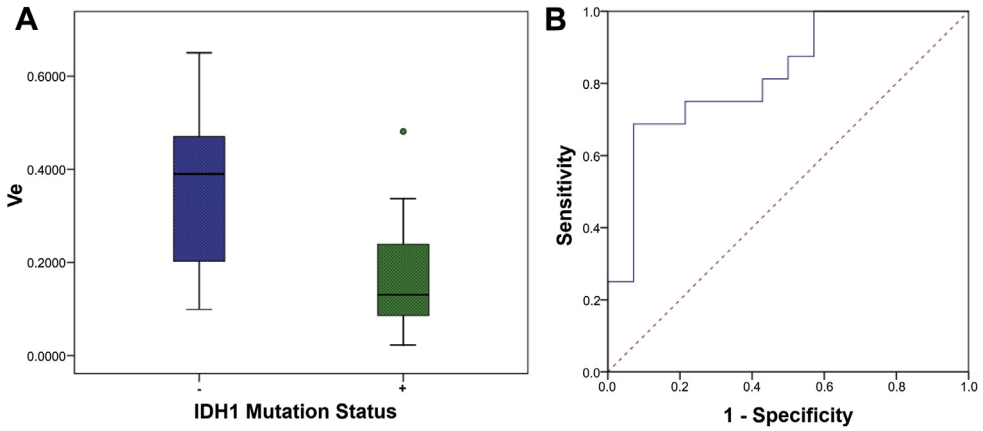

Figure 3. Boxplots of the best discriminatory dynamic contrast-enhanced T1-weighted perfusion magnetic resonance imaging (DCE-pMRI) parameters of volume of the extravascular extracellular space (fractional volume [%]) for the isocitrate dehydrogenase 1 (IDH1) mutation in the enhancing tumoral region of the glioblastomas (**A**). Receiver operating characteristic curve was used to compare the sensitivities and specificities of different quantitative DCE-pMRI parameters in glioblastomas. The discriminative power of DCE-pMRI parameters in the enhancing tumoral region for isocitrate dehydrogenase 1 mutation was highest for volume of the extravascular extracellular space with an area under the curve of 0.826 (**B**).

iAUC $\geq$0.2060, with sensitivity and specificity of 79.2 and 83.3%, respectively. According to the LOOCV of the iAUC, the cross-validated sensitivity and specificity in the prediction of EGFR amplification were 75.4% and 72.2%, respectively.

For NER, $MaxSlope_{NER}$ and $iAUC_{NER}$ of the GBs with EGFR amplification were significantly higher than those of the subgroup with EGFR amplification (after Bonferroni correction by a factor of 5, $MaxSlope_{NER}$, $P = 0.01$; $iAUC_{NER}$, $P = 0.025$) (Table 3 and Figure 6A), whereas there was no significant difference ($P > 0.05$) between patients with and without EGFR amplification with respect to the Kep_{NER}, $Ktrans_{NER}$, and Ve_{NER} values.

For the NER, the discriminative power of our individual imaging biomarkers was highest for $MaxSlope_{NER}$, with an AUC of 0.821 (Figure 6B). The GB with EGFR amplification could be differentiated from those without EGFR amplification by using $MaxSlope_{NER} \geq 0.0143$, with sensitivity and specificity of 83.3%

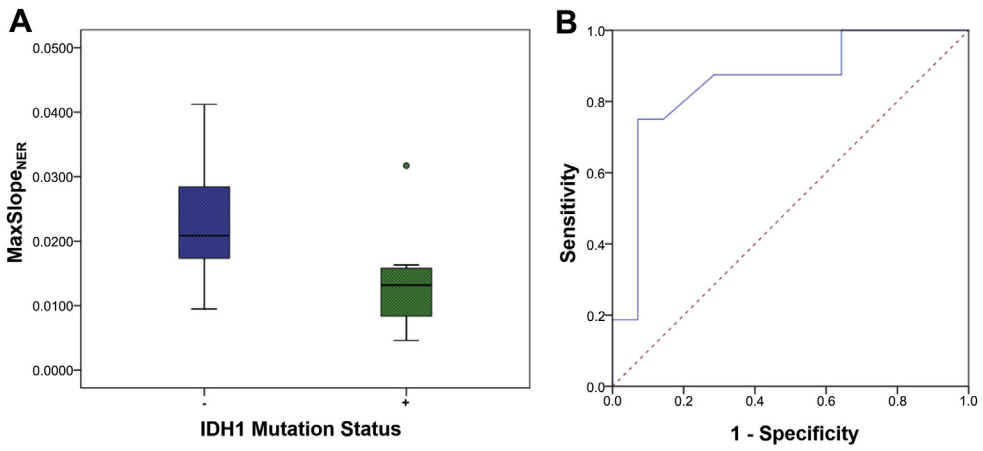

Figure 4. Boxplots of the best discriminatory dynamic contrast-enhanced T1-weighted perfusion magnetic resonance imaging (DCE-pMRI) parameters of $MaxSlope_{NER}$ for the isocitrate dehydrogenase 1 (IDH1) mutation in the nonenhancing peritumoral T2 hyperintense region of the glioblastomas (**A**). Receiver operating characteristic curve was used to compare the sensitivities and specificities of different quantitative DCE-pMRI parameters in glioblastomas. The discriminative power of DCE-pMRI parameters in the nonenhancing peritumoral T2 hyperintense region for isocitrate dehydrogenase 1 mutation was highest for maximum slope in the signal intensity-time series curve nonenhancing peritumoral T2 hyperintense region ($MaxSlope_{NER}$) with an area under the curve of 0.853 (**B**).

Table 3. Analysis of the Relationship Between Baseline Perfusion Parameters and Epidermal Growth Factor Receptor Amplification Status

		Dynamic Contrast-Enhanced T1-Weighted Perfusion Magnetic Resonance Imaging Parameters									
Epidermal Growth Factor Receptor Amplification Status		Initial Area Under Enhancement Curve	Initial Area Under Enhancement Curve Peritumoral Nonenhancing Region	Back Flux Constant (/minute)	Back Flux Constant Peritumoral Nonenhancing Region (/minute)	Transfer Constant (/minute)	Transfer Constant Peritumoral Nonenhancing Region (/minute)	Maximum Slope in Signal Intensity-Time Series Curve (/minute)	Maximum Slope Peritumoral Nonenhancing Region (/minute)	Volume of the Extravascular Extracellular Space (%)	Volume of the Extravascular Extracellular Space Peritumoral Nonenhancing Region (%)
–					N (n = 12)						
	Median	**0.113**	**0.060**	1.007	0.483	0.122	0.059	0.018	**0.011**	**0.092**	0.103
	Standard deviation	**0.099**	**0.055**	0.375	0.291	0.101	0.066	0.011	**0.006**	**0.149**	0.095
	Range	**0.313**	**0.204**	1.244	0.879	0.333	0.263	0.041	**0.023**	**0.436**	0.332
+					N (n = 24)						
	Median	**0.295**	**0.149**	0.986	0.941	0.250	0.125	0.029	**0.018**	**0.356**	0.184
	Standard deviation	**0.209**	**0.100**	0.824	0.552	0.265	0.194	0.026	**0.012**	**0.245**	0.180
	Range	**0.720**	**0.368**	3.235	1.839	1.147	0.961	0.092	**0.055**	**0.975**	0.825

Bold values mean *P* values of those parameters were <0.05 according to the Kruskal-Wallis test with Bonferroni correction.

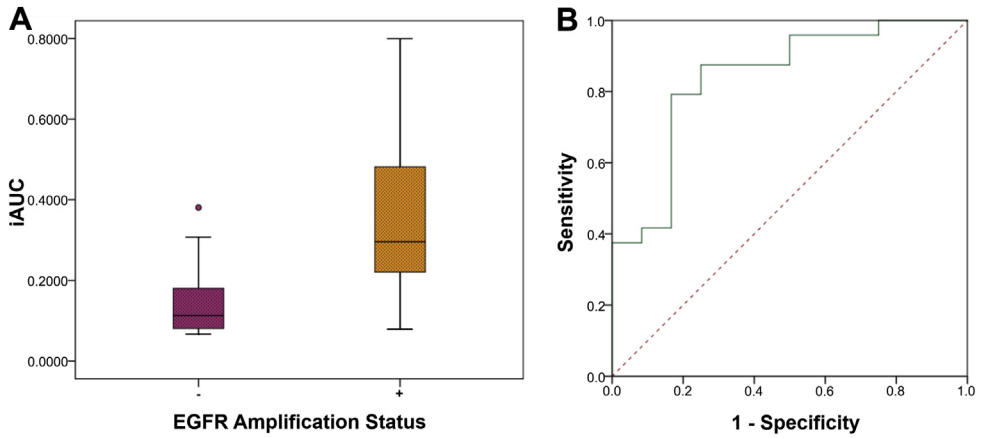

Figure 5. Boxplots of the best discriminatory dynamic contrast-enhanced T1-weighted perfusion magnetic resonance imaging (DCE-pMRI) parameters of initial area under enhancement curve for the epidermal growth factor receptor (EGFR) amplification in the enhancing tumoral region of the glioblastomas (**A**). Receiver operating characteristic curve was used to compare the sensitivities and specificities of different quantitative DCE-pMRI parameters in glioblastomas. The discriminative power of DCE-pMRI parameters in the enhancing tumoral region for epidermal growth factor receptor amplification was highest for initial area under enhancement curve (iAUC) with an area under the curve of 0.840 (**B**).

and 75%, respectively. According to the LOOCV of the $MaxSlope_{NER}$, the cross-validated sensitivity and specificity in the prediction of EGFR amplification were 78.7% and 68.3%, respectively.

OLIG2 Expression

The Ktrans and Kep parameters of the GBs without OLIG2 expression in the ER were significantly higher than those of the subgroup with OLIG2 expression (after Bonferroni correction by a factor of 5, Ktrans, $P = 0.03$; Kep, $P = 0.04$) (Table 4 and Figure 7A). In terms of iAUC, MaxSlope, and Ve parameters gathered from ER, we found no significant difference between the groups with OLIG2 mutation and without OLIG2 mutation ($P > 0.05$).

For the ER, the discriminative power of our individual imaging biomarkers was highest for Ktrans, with an AUC of 0.837

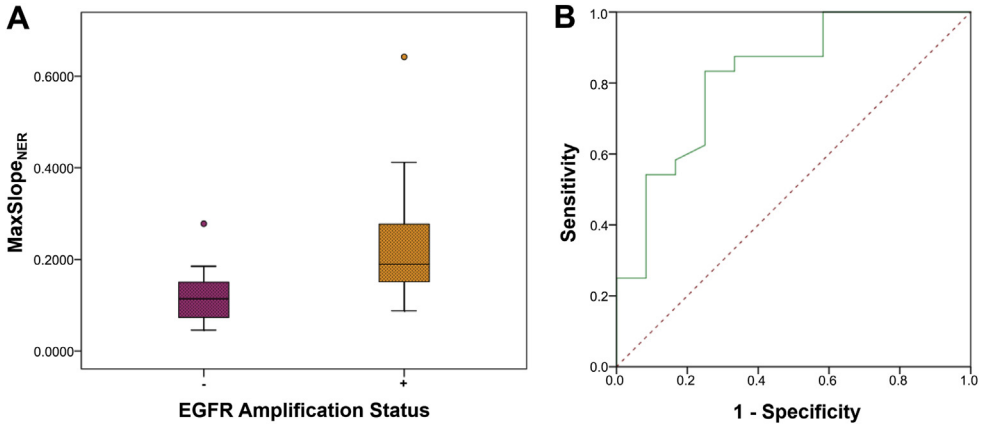

Figure 6. Boxplots of the best discriminatory dynamic contrast-enhanced T1-weighted perfusion magnetic resonance imaging (DCE-pMRI) parameters of maximum slope in the signal intensity-time series curve nonenhancing peritumoral T2 hyperintense region ($MaxSlope_{NER}$) for the epidermal growth factor receptor (EGFR)amplification in the nonenhancing peritumoral T2 hyperintense region of the glioblastomas (**A**). Receiver operating characteristic curve was used to compare the sensitivities and specificities of different quantitative DCE-pMRI parameters in glioblastomas. The discriminative power of DCE-pMRI parameters in the nonenhancing peritumoral T2 hyperintense region for epidermal growth factor receptor amplification was highest for $MaxSlope_{NER}$ with an area under the curve of 0.821 (**B**).

Table 4. Analysis of the Relationship Between Baseline Perfusion Parameters and Oligodendrocyte Transcription Factor 2expression Status

Oligodendrocyte Transcription Factor 2 Expression Status		Dynamic Contrast-Enhanced T1-Weighted Perfusion Magnetic Resonance Imaging Parameters									
		Initial Area Under Enhancement Curve	Initial Area Under Enhancement Curve Peritumoral Nonenhancing Region	Back Flux Constant (/minute)	Back Flux Constant Peritumoral Nonenhancing Region (/minute)	Transfer Constant (/minute)	Transfer Constant Peritumoral Nonenhancing Region (/minute)	Maximum Slope in Signal Intensity-Time Series Curve (/minute)	Maximum Slope Peritumoral Nonenhancing Region (/minute)	Volume of the Extravascular Extracellular Space (%)	Volume of the Extravascular Extracellular Space Peritumoral Nonenhancing Region (%)
−	N (n = 7)										
	Median	0.414	0.157	**1.491**	0.414	**0.540**	0.151	0.042	0.015	0.333	0.169
	Standard deviation	0.276	0.131	**0.936**	0.544	**0.354**	0.327	0.032	0.019	0.347	0.288
	Range	0.665	0.368	**2.647**	1.309	**1.059**	0.911	0.091	0.055	0.937	0.825
+	N (n = 29)										
	Median	0.236	0.085	**0.815**	0.740	**0.170**	0.083	0.021	0.016	0.247	0.130
	Standard deviation	0.170	0.081	**0.568**	0.519	**0.147**	0.089	0.020	0.009	0.189	0.110
	Range	0.679	0.319	**2.263**	1.839	**0.638**	0.269	0.083	0.036	0.627	0.435

Bold values mean *P* values of those parameters were <0.05 according to the Kruskal-Wallis test with Bonferroni correction.

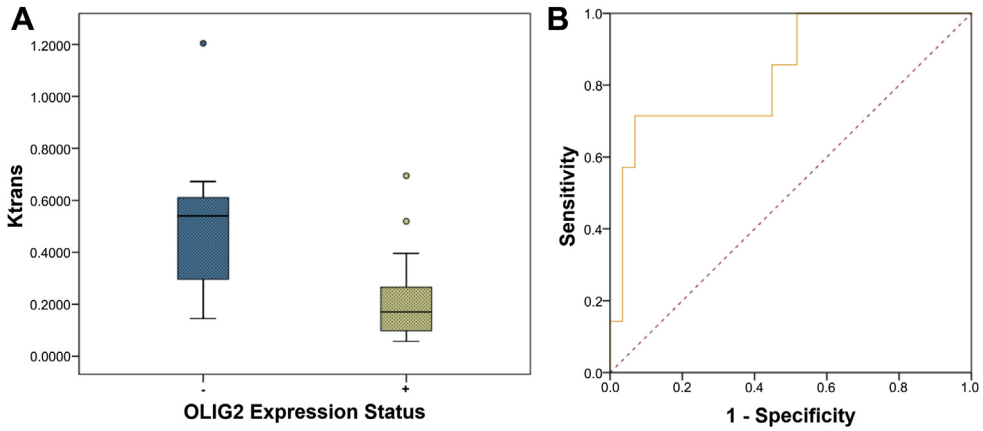

Figure 7. Boxplots of the best discriminatory dynamic contrast-enhanced T1-weighted perfusion magnetic resonance imaging (DCE-pMRI) parameter of forward volume transfer constant (Ktrans) for the oligodendrocyte transcription factor 2 (OLIG2) expression in the enhancing tumoral region of the glioblastomas (**A**). Receiver operating characteristic curve was used to compare the sensitivities and specificities of different quantitative DCE-pMRI parameters in glioblastomas. The discriminative power of DCE-pMRI parameters in the enhancing tumoral region for oligodendrocyte transcription factor 2 expression was highest for forward volume transfer constant with an area under the curve of 0.837 (**B**).

(Figure 7B). The GB with OLIG2 expression could be differentiated from those without OLIG2 expression by using Ktrans ≤0.3962, with sensitivity and specificity of 71.4% and 93.1%, respectively. According to the LOOCV of the Ktrans, the cross-validated sensitivity and specificity in the prediction of OLIG2 expression were 67.8% and 83.2%, respectively.

However, there were no significant differences in all DCE-pMRI values among the groups with different OLIG2 expression status for NER ($P > 0.05$).

Ki-67 Labeling Index and p53 Mutation

The Ki-67 labeling index presented a strong positive correlation with iAUC ($r = 0.619$; $P < 0.001$); a moderate positive correlation with $iAUC_{NER}$ ($r = 0.524$; $P = 0.01$), Kep ($r = 0.492$; $P = 0.02$), Ktrans ($r = 0.596$; $P < 0.001$), $Ktrans_{NER}$ ($r = 0.465$; $P = 0.04$), Ve ($r = 0.540$; $P = 0.01$), and Ve_{NER} ($r = 0.530$; $P = 0.01$) (all after Bonferroni correction by a factor of 10) (Figure 8).

The sensitivity and specificity were calculated for a number of Ki-67 labeling index cutoff values and the expression level of Ki-67 index was graded as high (≥30%) or low (<30%) level for further analysis based on the highest Youden index. The discriminative power of our individual imaging biomarkers was highest for iAUC, with an AUC of 0.75. The GBs with high Ki-67 labeling index could be differentiated from GBs with low Ki-67 labeling index by using iAUC ≥0.172, with sensitivity and specificity of 88.8% and 61.1%, respectively.

The p53 gene expression status did not present a significant correlation with the DCE-pMRI values ($P > 0.05$).

The interobserver agreement for the quantitative analysis of SI was almost perfect for all DCE-pMRI values (range, 0.90–0.99; 95% confidence interval, 0.85–1.00). Intraobserver agreements for quantitative imaging parameters ranged from 0.85 to 0.95 for both readers (intraclass correlation coefficients).

DISCUSSION

GB, the most aggressive subtype of glioma, has high vascularization and diverse genetic alterations.[22] Molecular subtypes of GB have distinct prognoses and also potentially different susceptibility to specific treatments.[3] Therefore, noninvasive surrogates for IHC biomarkers of GB might be clinically beneficial. In our study, we directly correlated DCE-pMRI findings with clinically important IHC markers of angiogenesis in GB. We found that various

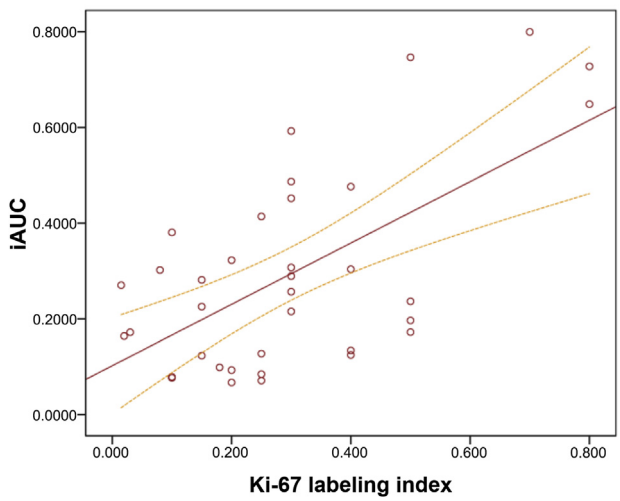

Figure 8. Scatter diagram and regression line display the relationship between initial area under enhancement curve (iAUC) and Ki-67 labeling index. Ki-67 labeling index revealed a strong positive correlation with initial area under enhancement curve ($r = 0.619$; $P < 0.001$).

quantitative and semi-quantitative DCE-pMRI parameters acquired from the ER and NER were significantly correlated with surrogate IHC biomarkers of GB, such as EGFR amplification, IDH1 mutation, and OLIG2 expression. In addition, the Ki-67 labeling index indicated a significant positive correlation with most of the DCE-pMRI parameters. These findings support our initial hypothesis that GB with different IHC biomarkers may have unique imaging phenotypes.

In distinguishing genetic biomarkers of GBs with the DCE-pMRI–derived parameters, special interest was given to NER, because NER is a combination of infiltrative tumor cells and vasogenic edema, and the former might directly contribute to a local recurrence.[23] $MaxSlope_{NER}$, Ve_{NER}, and $iAUC_{NER}$ parameters derived from NER of IDH-wt GB were statistically higher than in IDH-mut GB in our series. This finding might be attributed to various factors, particularly to cortical disruption and brain invasion,[24] which might be more common in IDH-wt GB than in IDH-mut GB and might result in richer peritumoral blood supply. Our results showed that the correlation between DCE-pMRI parameters and genetic mutations were different in the ER and NER of the GBs. This finding suggests different perfusion associations in the ER and NER of GB, and that the genomic mechanisms of angiogenesis in GB may be heterogeneous.

pMRI is one of the most effective noninvasive methods for quantifying neoplastic neovascularization. Various quantitative and semi-quantitative DCE-pMRI parameters may provide valuable information about tumor angiogenesis and permeability.[25] DCE-pMRI–derived Ktrans, the volume transfer constant of contrast agent from a plasma space to an EES, reflects both flow and vascular permeability within brain tissue.[26] It, therefore, can reflect the neoangiogenic nature of the tumor microvasculature. Ve is the volume fraction of the contrast agent leaking into the EES, which is a marker of cell density and reflects the abnormal architecture of the tumor tissue. Theoretically, tumors with aggressive behavior are expected to show higher values of Ktrans and Ve as a result of higher endothelial permeability and blood volume, respectively.[27] Kep was defined as reverse reflux rate of the contrast agent from an EES to a plasma space. The Kep parameter could reflect the destruction of the blood-brain barrier as well as the pressure of the tissue around the tumor.[28] Theoretically, it is expected that in GBs without OLIG2 expression, the tissue pressure around the tumor could be increased because OLIG2 expression–negative cells grow as clusters around blood vessels and express high levels of the vascular endothelial growth factor (VEGF). Compatibly, the Kep parameter in GB without OLIG2 expression was increased in our series. The iAUC is a different pathophysiologic factor in a model-free approach, which is a semi-quantitative factor that measures the total amount of contrast agent inflow to and remaining in the tumor tissue.[29] The initial MaxSlope on iAUC shows the early vascular phase, which derives mainly from the early leakage of contrast agent into the EES caused by a defective blood-brain barrier.[18] Therefore, GBs with aggressive molecular alterations may have a higher MaxSlope as a result of a prominent early vascular phase based on hypervascularity and neoangiogenesis.

The need for less-invasive methods for the detection of the major molecular alterations in GB has led radiologists to search for imaging biomarkers reflecting genetic profiles of GB. Several studies have shown the association of molecular glioma markers with specific tumoral imaging characteristics.[30] Studies by Arevalo-Perez et al.[31] and Tykocinski et al.[32] showed that EGFRvIII-expressing GBs showed significantly higher relative tumor blood volume (TBV) compared with those tumors with deficient EGFRvIII expression. The major genetic alterations in GBs were also evaluated by dynamic susceptibility contrast MRI by Ryoo et al.,[33] which analyzed phosphatase and tensin homologue, EGFR, Ki-67 labeling index, O_6-methylguanine methyltransferase, and p53 mutation for correlation with the TBV. These investigators determined that GBs having aggressive genetic alterations tended to have a higher TBV. To study the perfusion effects of IDH, Kickingereder et al.[34] analyzed 288 patients with glioma and showed that a 1-unit increase in relative cerebral blood volume corresponded to a two thirds decrease in the odds for an IDH mutation and accurately predicted IDH-mut GBs in 88% of patients. Besides, other studies have focused on peripheral edema of GB. Akbari et al.[35] and Jain et al.[23] studied the NER of GB to account for heterogeneity and possible tumor infiltration in the peripheral edema. These investigators have suggested that NER of GBs could have important imaging phenotypic features that are complementary to clinical and genomic features and can improve models of patient prognosis. Liu et al.[19] analyzed 41 patients with GB and suggested that subtype-specific treatment of NER might be substantial because, in their study, the association between imaging parameters and genomic biomarkers was different in ER and NER of GB. However, studies correlating DCE-pMRI characteristics in the ER and NER with major IHC biomarkers of GB have not yet been conducted.

Study Limitations

This pilot study was the retrospective result of an exploratory analysis; therefore, it has several limitations. First, the sample size was relatively small to generalize our findings. Furthermore, DCE-pMRI parameters showed only borderline significance for OLIG2 expression and EGFR amplification on the LOOCV test and lacked sensitivity for IDH1 mutation. This result may also be attributed to our small sample size. The limited number of patients in this study does not permit us to draw any firm conclusions about those perfusion parameters that were able to determine the IHC biomarkers of GBs. These DCE-pMRI parameters should be investigated in multicenter prospective studies with large numbers of patients. Second is a lack of generalizability and standardization of DCE-MRI-derived parameters, which can be affected by post-processing software, and the protocol of DCE-MRI. Therefore, any specific cutoff values of perfusion parameters in our study could not be generally applied to those from other institutions. Third, we did not analyze the impact of EGFRvIII, O_6-methylguanine methyltransferase, and phosphatase and tensin homologue mutations, which are also known to have an impact on perfusion parameters as well as VEGF levels, which could be directly correlated with the neovascularization of the tumor tissue. The degree of perfusion abnormality reflects the degree of tumor microvascularity, not the IHC biomarkers of GB directly, and consequently, additional studies may clarify the relationship between the VEGF, perfusion abnormalities, and molecular subtypes of GB. The tumor tissue used for IHC analysis was resected from T1-enhancing solid regions. We could not evaluate the exact

association between DCE-pMRI and genomics changes in the NER of GB, because we did not acquire tissues from NER. Also, IHC may not capture all IDH1 mutations, meaning that the cohort might have a slightly different incidence of IDH1 mutation–positive tumors than reported in our study. Whereas genome sequencing might have provided a more definitive method for determining IDH1 mutation status, this type of confirmatory investigation is required for genetic analysis but was not performed in the present study. Future studies with larger samples and prospective approaches to enable the direct correlation of imaging with histologic observations are warranted to further investigate the diagnostic potential of the presented imaging approach.

CONCLUSIONS

Although the relatively small sample size of this retrospective pilot study cautions against overinterpretation, our results suggest that DCE-pMRI may serve as a noninvasive and easily accessible method to predict certain IHC biomarkers of GB. However, histopathologic analysis with genome sequencing is still the gold standard in confirming genetic profiles.

REFERENCES

1. Xu H, Chen J, Xu H, Qin Z. Geographic variations in the incidence of glioblastoma and prognostic factors predictive of overall survival in US adults from 2004-2013. *Front Aging Neurosci*. 2017;9:352.
2. Thakkar JP, Dolecek TA, Horbinski C, Ostrom QT, Lightner DD, Barnholtz-Sloan JS, et al. Epidemiologic and molecular prognostic review of glioblastoma. *Cancer Epidemiol Biomarkers Prev*. 2014;23:1985-1996.
3. Cancer Genome Atlas Research N. Comprehensive genomic characterization defines human glioblastoma genes and core pathways. *Nature*. 2008;455:1061-1068.
4. Zhang GB, Cui XL, Sui DL, Ren XH, Zhang Z, Wang ZC, et al. Differential molecular genetic analysis in glioblastoma multiforme of long- and short-term survivors: a clinical study in Chinese patients. *J Neurooncol*. 2013;113:251-258.
5. Furnari FB, Fenton T, Bachoo RM, Mukasa A, Stommel JM, Stegh A, et al. Malignant astrocyticglioma: genetics, biology, and paths to treatment. *Genes Dev*. 2007;21:2683-2710.
6. Wang PF, Song HW, Cai HQ, Kong LW, Yao K, Jiang T, et al. Preoperative inflammation markers and IDH mutation status predict glioblastoma patient survival. *Oncotarget*. 2017;8:50117-50123.
7. Zeng A, Hu Q, Liu Y, Wang Z, Cui X, Li R, et al. IDH1/2 mutation status combined with Ki-67 labeling index defines distinct prognostic groups in glioma. *Oncotarget*. 2015;6:30232-30238.
8. Trépant AL, Bouchart C, Rorive S, Sauvage S, Decaestecker C, Demetter P, et al. Identification of OLIG2 as the most specific glioblastoma stem cell marker starting from comparative analysis of data from similar DNA chip microarray platforms. *Tumour Biol*. 2015;36:1943-1953.
9. Alton G, Kesari S. Novel small molecule inhibitors of the OLIG2 transcription factor: promising new therapeutics for glioblastoma. *Future Oncol*. 2016;12:1001-1004.
10. von Achenbach C, Weller M, Szabo E. Epidermal growth factor receptor and ligand family expression and activity in glioblastoma. *J Neurochem*. 2018;147:99-109.
11. Felsberg J, Hentschel B, Kaulich K, Gramatzki D, Zacher A, Malzkorn B, et al. Epidermal growth factor receptor variant III (EGFRvIII) positivity in EGFR-amplified glioblastomas: prognostic role and comparison between primary and recurrent tumors. *Clin Cancer Res*. 2017;23:6846-6855.
12. Padfield E, Ellis HP, Kurian KM. Current therapeutic advances targeting EGFR and EGFRvIII in glioblastoma. *Front Oncol*. 2015;5:5.
13. Kickingereder P, Neuberger U, Bonekamp D, Piechotta PL, Götz M, Wick A, et al. Radiomic subtyping improves disease stratification beyond key molecular, clinical, and standard imaging characteristics in patients with glioblastoma. *Neuro Oncol*. 2018;20:848-857.
14. Hong EK, Choi SH, Shin DJ, Jo SW, Yoo RE, Kang KM, et al. Radiogenomics correlation between MR imaging features and major genetic profiles in glioblastoma. *Eur Radiol*. 2018;28:4350-4361.
15. Santarosa C, Castellano A, Conte GM, Cadioli M, Iadanza A, Terreni MR, et al. Dynamic contrast-enhanced and dynamic susceptibility contrast perfusion MR imaging for glioma grading: preliminary comparison of vessel compartment and permeability parameters using hotspot and histogram analysis. *Eur J Radiol*. 2016;85:1147-1156.
16. Jung SC, Yeom JA, Kim JH, Ryoo I, Kim SC, Shin H, et al. Glioma: application of histogram analysis of pharmacokinetic parameters from T1-weighted dynamic contrast-enhanced MR imaging to tumor grading. *AJNR Am J Neuroradiol*. 2014;35:1103-1110.
17. Kickingereder P, Sahm F, Wiestler B, Roethke M, Heiland S, Schlemmer HP, et al. Evaluation of microvascular permeability with dynamic contrast-enhanced MRI for the differentiation of primary CNS lymphoma and glioblastoma: radiologic-pathologic correlation. *AJNR Am J Neuroradiol*. 2014;35:1503-1508.
18. Xie T, Chen X, Fang J, Kang H, Xue W, Tong H, et al. Textural features of dynamic contrast-enhanced MRI derived model-free and model-based parameter maps in glioma grading. *J Magn Reson Imaging*. 2018;47:1099-1111.
19. Liu X, Mangla R, Tian W, Qiu X, Li D, Walter KA, et al. The preliminary radiogenomics association between MR perfusion imaging parameters and genomic biomarkers, and their predictive performance of overall survival in patients with glioblastoma. *J Neurooncol*. 2017;135:553-560.
20. Cui Y, Ren S, Tha KK, Wu J, Shirato H, Li R. Volume of high-risk intratumoral subregions at multi-parametric MR imaging predicts overall survival and complements molecular analysis of glioblastoma. *Eur Radiol*. 2017;27:3583-3592.
21. Tofts PS, Kermode AG. Measurement of the blood-brain barrier permeability and leakage space using dynamic MR imaging. 1. Fundamental concepts. *Magn Reson Med*. 1991;17:357-367.
22. Ohgaki H, Kleihues P. Genetic pathways to primary and secondary glioblastoma. *Am J Pathol*. 2007;170:1445-1453.
23. Jain R, Poisson LM, Gutman D, Scarpace L, Hwang SN, Holder CA, et al. Outcome prediction in patients with glioblastoma by using imaging, clinical, and genomic biomarkers: focus on the nonenhancing component of the tumor. *Radiology*. 2014;272:484-493.
24. Masui K, Kato Y, Sawada T, Mischel P, Shibata N. Molecular and genetic determinants of glioma cell invasion. *Int J Mol Sci*. 2017;18:E2609.
25. Tietze A, Mouridsen K, Lassen-Ramshad Y, Østergaard L. Perfusion MRI derived indices of microvascular shunting and flow control correlate with tumor grade and outcome in patients with cerebral glioma. *PLoS One*. 2015;10:e0123044.
26. Taoka T, Kawai H, Nakane T, Hori S, Ochi T, Miyasaka T, et al. Application of histogram analysis for the evaluation of vascular permeability in glioma by the K2 parameter obtained with the dynamic susceptibility contrast method: comparisons with Ktrans obtained with the dynamic contrast enhance method and cerebral blood volume. *Magn Reson Imaging*. 2016;34:896-901.
27. Mills SJ, Du Plessis D, Pal P, Thompson G, Buonacorrsi G, Soh C, et al. Mitotic activity in glioblastoma correlates with estimated extravascular extracellular space derived from dynamic contrast-enhanced MR imaging. *AJNR Am J Neuroradiol*. 2016;37:811-817.
28. Kickingereder P, Wiestler B, Graf M, Heiland S, Schlemmer HP, Wick W, et al. Evaluation of dynamic contrast-enhanced MRI derived microvascular permeability in recurrent glioblastoma treated with bevacizumab. *J Neurooncol*. 2015;121:373-380.
29. Choi YS, Lee HJ, Ahn SS, Chang JH, Kang SG, Kim EH, et al. Primary central nervous system lymphoma and atypical glioblastoma:

differentiation using the initial area under the curve derived from dynamic contrast-enhanced MR and the apparent diffusion coefficient. *Eur Radiol*. 2017;27:1344-1351.

30. Naeini KM, Pope WB, Cloughesy TF, Harris RJ, Lai A, Eskin A, et al. Identifying the mesenchymal molecular subtype of glioblastoma using quantitative volumetric analysis of anatomic magnetic resonance images. *Neuro Oncol*. 2013;15:626-634.

31. Arevalo-Perez J, Thomas AA, Kaley T, Lyo J, Peck KK, Holodny AI, et al. T1-weighted dynamic contrast-enhanced MRI as a noninvasive biomarker of epidermal growth factor receptor vIII status. *AJNR Am J Neuroradiol*. 2015;36:2256-2261.

32. Tykocinski ES, Grant RA, Kapoor GS, Krejza J, Bohman LE, Gocke TA, et al. Use of magnetic perfusion-weighted imaging to determine epidermal growth factor receptor variant III expression in glioblastoma. *Neuro Oncol*. 2012;14:613-623.

33. Ryoo I, Choi SH, Kim JH, Sohn CH, Kim SC, Shin HS, et al. Cerebral blood volume calculated by dynamic susceptibility contrast-enhanced perfusion MR imaging: preliminary correlation study with glioblastoma genetic profiles. *PLoS One*. 2013;8:e71704.

34. Kickingereder P, Sahm F, Radbruch A, Wick W, Heiland S, Von Deimling A, et al. IDH mutation status is associated with a distinct hypoxia/angiogenesis transcriptome signature which is non-invasively predictable with rCBV imaging in human glioma. *Sci Rep*. 2015;5:16238.

35. Akbari H, Macyszyn L, Da X, Bilello M, Wolf RL, Martinez-Lage M, et al. Imaging surrogates of infiltration obtained via multiparametric imaging pattern analysis predict subsequent location of recurrence of glioblastoma. *Neurosurgery*. 2016;78:572-580.

Conflict of interest statement: The authors declare that the article content was composed in the absence of any commercial or financial relationships that could be construed as a potential conflict of interest.

Received 21 February 2019; accepted 9 April 2019

Citation: World Neurosurg. (2019) 128:e195-e208.
https://doi.org/10.1016/j.wneu.2019.04.089

Journal homepage: ***www.journals.elsevier.com/world-neurosurgery***

Available online: ***www.sciencedirect.com***